Multi-scale analysis of mechanical properties and damage behavior of polypropylene composite (GF50-PP) plate at room and cryogenic temperatures

Mohammadali Shirinbayan, Mojdeh Rezaei-Khamseh, Mohammad Hossein Nikooharf, Abbas Tcharkhtchi

▶ **To cite this version:**

Mohammadali Shirinbayan, Mojdeh Rezaei-Khamseh, Mohammad Hossein Nikooharf, Abbas Tcharkhtchi. Multi-scale analysis of mechanical properties and damage behavior of polypropylene composite (GF50-PP) plate at room and cryogenic temperatures. Composite Structures, 2021, 278, pp.114713. 10.1016/j.compstruct.2021.114713 . hal-03382411

HAL Id: hal-03382411
https://hal.science/hal-03382411

Submitted on 18 Oct 2021

HAL is a multi-disciplinary open access archive for the deposit and dissemination of scientific research documents, whether they are published or not. The documents may come from teaching and research institutions in France or abroad, or from public or private research centers.

L'archive ouverte pluridisciplinaire **HAL**, est destinée au dépôt et à la diffusion de documents scientifiques de niveau recherche, publiés ou non, émanant des établissements d'enseignement et de recherche français ou étrangers, des laboratoires publics ou privés.

Multi-scale analysis of mechanical properties and damage behavior of polypropylene composite (GF50-PP) plate at room and cryogenic temperatures

Mohammadali Shirinbayan *, Mojdeh Rezaei-khamseh, Mohammad Hossein Nikooharf, Abbas Tcharkhtchi, Joseph Fitoussi

Arts et Metiers Institute of Technology, CNAM, PIMM, HESAM University, F-75013 Paris, France

ARTICLE INFO

Keywords:
Glass fiber-reinforced composite
Cryogenic temperature
Fatigue
Damage
Plasticity

ABSTRACT

In this paper, glass fiber-reinforced polypropylene (GF50-PP) composite composed of long fibers was prepared by the thermo-compression process for the very first time. This composite presents high mechanical strength and is used in infrastructures, which demand resistance against severe conditions. Mechanical strength and multi-scale damage analysis of GF50-PP composite at ambient and cryogenic temperatures have been investigated in this study using a special sampling procedure according to the microscopy observation, X-ray microtomography, ultrasonic measurement, and pyrolysis. The results demonstrated the exceptional behavior of the GF50-PP at the cryogenic temperature of −70 °C mainly due to the employment of a novel processing method (thermo-compression) for composites with long fibers, which have been previously prepared by traditional injection molding process. Tensile results presented no difference in failure strain at 20 °C and −70 °C and the fatigue lifetime for different fiber orientations was similar in 3-points bending fatigue tests for different orientations of fibers or in samples taken from different regions of the composite plate, indicating the efficinecy of this processing method. Moreover, the results of damage analysis through monotonic loading presented that by decreasing the temperature from 20 °C to −70 °C, the plasticity threshold didn't change notably. Overall, the proposed preparation method provided outstanding uniformity and excellent mechanical properties in GF50-PP composite even at temperatures as low as −70 °C, which has not been investigated at this cryogenic temperature before.

1. Introduction

Long glass fiber-reinforced thermoplastic composites are attracting widespread interest on account of their reliable mechanical properties and high specific strength, formability, and lightweight for a wide range of industrial applications including automotive, aerospace, marine, and petroleum industries [1]. Long fiber-reinforced composites are capable of withstanding severe conditions, particularly pressure or temperature variations [2,3].

Polypropylene is largely used as a matrix for long glass fibers owing to its low density, good physical and mechanical properties, convenient processing characteristics, high chemical and thermal stability as well as cost-effectiveness [4–6]. Glass fiber-reinforced PP composites present excellent strength, high flexibility, convenient impact properties, high thermal resistance as well as good recyclability and lightweight, which have made them to be widely used in automotive, pipe, marine, military and aerospace industries [7–15].

Thermo-compression molding, especially used in the automotive industry, is one of the simplest and most cost-effective processing methods for large-scale production of long fiber-reinforced composites, which facilitates embedding longer glass fibers inside the polymeric matrix compared with injection molding and extrusion processes, which are traditionally used for preparing fiber-reinforced composites. This process includes heating fiber-reinforced thermoplastics above melting temperature to initiate the material flow followed by mold filling and hot-pressing. The cooling phase is the final step in this process [16–18]. Fiber-reinforced composites are exposed to a variety of complex effects during thermo-compression molding, which can lead to specific fiber

* Corresponding author.
E-mail addresses: mohammadali.shirinbayan@ensam.eu (M. Shirinbayan), mohammad_hossein.nikooharf_tamiz@ensam.eu (M.H. Nikooharf), abbas.tcharkhtchi@ensam.eu (A. Tcharkhtchi), joseph.fitoussi@ensam.eu (J. Fitoussi).

orientation, fiber-matrix separation, and fiber distribution. These phenomena would affect the mechanical properties of the composite [19,20]. As a consequence, the final mechanical properties and damage behavior of these composites should be thoroughly examined in order to predict their behavior and ensure their performance, especially at cryogenic temperatures, at which materials are mostly supposed to present inferior mechanical properties and damage behavior.

There is a vast amount of literature on the visco-elasto-plastic behavior, mechanical properties and damage analysis of polymer-based glass fiber composites. For instance, In a study carried out by Achour et al. [21,22] on polypropylene filled with different levels of glass fiber (30%, 40%, 60%) and at strain rates ranging from $4 \times 10^{-4}\ s^{-1}$ to $100\ s^{-1}$, an increase in Young's modulus and stress at break of up to 100% and an increase of 200% to 300% in damage threshold stresses have been mentioned. Another study carried out by Fitoussi et al. [23] on the multi-scale analysis of glass fiber-reinforced ethylene-propylene copolymer (EPC) composites demonstrated that the effect of strain rate on the damage behavior of EPC matrix composite is primarily a result of the viscous behavior of the EPC matrix. By increasing the strain rate, the local deformation zone encompassing the fibers acts as a dissipation zone, and the damage initiation is delayed. The same finding was reported by Jendli et al. [24,25] for thermoset composites. In addition, Bonnet [26] studied the effect of strain rate on the mechanical behavior of polypropylene composite reinforced by 30 wt% glass fiber. Over a strain rate range from $10^{-1}\ s^{-1}$ to $200\ s^{-1}$, the author noted a significant increase in the threshold stresses of plasticity and damage with the strain rate. They also remarked a saturation in the viscoelastic effects. In general, it seems that the strain rate has a strong influence on the mechanical behavior of polymer materials. It can be noted that the increase in the stress at break and stiffness, reduction of the strain at break, increased damage and plasticity thresholds and saturation of the viscoelastic effects are among the most important consequences of high strain rate [27–29].

On the other hand, a great deal of attention must be paid while setting fatigue test process parameters. For instance, high load cycle frequency would lead to a self-heating phenomenon causing the matrix to transform from a glassy to a rubbery state and to decrease modulus [30,31]. In this manner, Zhou and Mallick [32,33] studied the effect of frequency on the fatigue life of glass fiber polyamide composite. They have noted that for frequencies between 0.5 Hz and 2 Hz, the increase in frequency improves the mechanical fatigue life. In contrast, for frequencies between 2 and 20 Hz, thermal fatigue would be significant. Esmaeillou et al. [34] also studied a glass fiber-reinforced polyamide composite in frequencies between 20 Hz and 60 Hz during the tension–tension fatigue test. They have reported that at low frequencies, mechanical fatigue is dominant while at high frequencies mechanical and thermal fatigue coupling are observable.

Several damage mechanisms can take place in a composite structure, depending on the composition of the composite material and the type of loading. Generally, the degradation of composite materials begins at the microscopic scale when local stresses at the fiber–matrix interface reach a certain threshold value. This may lead to matrix microcracking, delamination of the fiber–matrix interfaces, fiber breaks, etc. The macroscopic damage is initiated at a stress around 25–40% of the ultimate stress value and results in a loss of material stiffness [28,35,36]. In this regard, Arif et al. [37] used in-situ microtopography technique combined with SEM observations on glass fiber-reinforced PA66 composite at different humidity levels to investigate damage mechanisms. They have mentioned the following damage mechanism: (1) the initiation of damage appears in the form of fiber–matrix delamination at fiber tips, specifically where the fibers are close to each other due to stress concentration, (2) propagation of Interfacial delamination along the fiber–matrix interfaces with occasional fiber breakages, (3) the appearance of matrix microcracks, and (4) the propagation of matrix microcracks leading to an accumulation of damage and the collapse of the material. Rolland et al. [38,39] also studied the fatigue damage of

Table 1
GF50-PP composition.

Product nature	Composition (wt%)
Glass fibers	50%
Polypropylene	50%

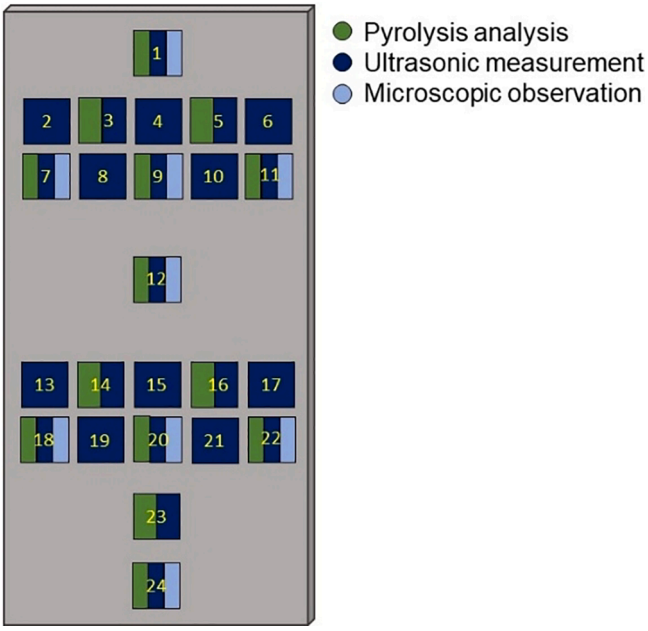

Fig. 1. Sampling schematic of the GF50-PP composite for pyrolysis analysis, ultrasonic measurements and microscopic observations.

PA66-based composite using in situ X-ray micro-tomographic analysis. They concluded that cavitation plays an important role in fatigue damage and suggested that cavitation triggers other damage phenomena.

Many theoretical models have also been developed in order to study fatigue damage for explaining the behaviour of fatigue cracks. For instance, Sun et al. [40] have proposed a multi-scale fatigue damage model to investigate the nucleation and growth behaviour of short fatigue cracks and the evolution of fatigue damage in micro-scale and macro-scale, respectively. The model was capable of predicting the fatigue life through fatigue damage accumulation. The same authors [41] have additionally developed a multi-scale fatigue model as well as an image-based simulation route for explaining collective short cracks evolution process and continuous fatigue damage evolution in micro-scale and macro-scale based on the continuum damage mechanics (CDM) in order to conceive the mechanisms of fatigue phenomenon [42,43].

It is worth mentioning that by cooling the material down to cryogenic temperatures, unequal coefficients of thermal expansion between the fibers and the matrix would cause significant internal stresses that would eventually initiate the formation of microcracks in the polymer matrix [44].

In order to achieve highly reliable properties of fiber-reinforced composites, a profound comprehension of the damage mechanisms under hydrostatic stress, impact behavior, mechanical and thermal fatigue behavior at ambient, elevated, and cryogenic temperatures, as well as aging and environmental degradation conditions would be necessary. In addition, for achieving optimized macroscopic behavior and desired microstructural characteristics, it would be crucial to understand the phenomena of the evolution of process variables and process-related composite characteristics, in which the process history must be carefully evaluated. Aiming for these goals, a thorough investigation of

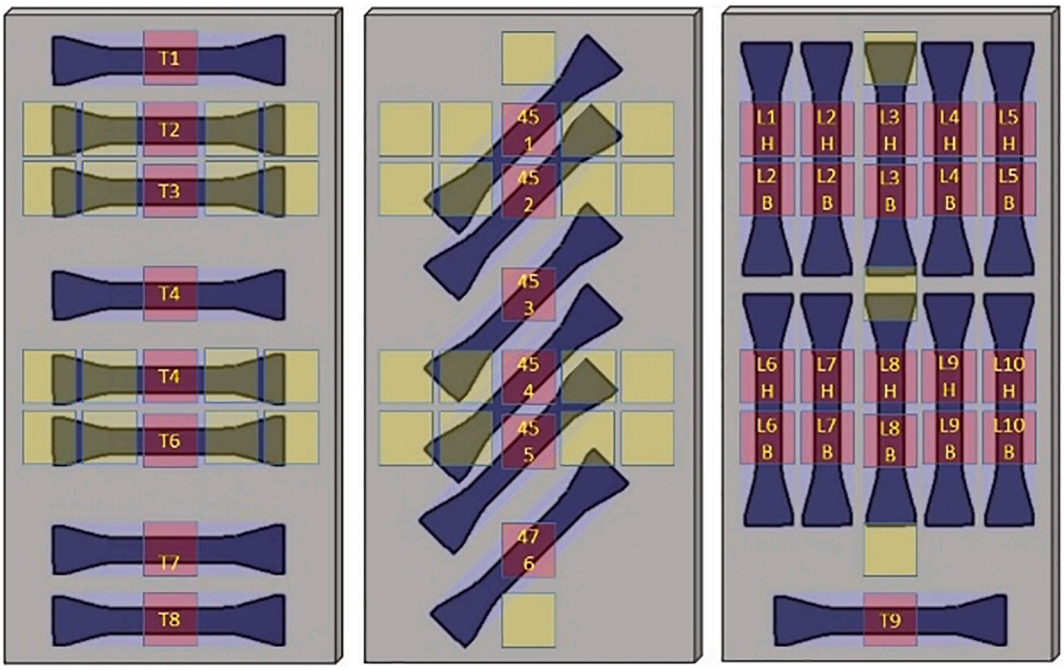

Fig. 2. Sampling procedure of the GF50-PP composite for mechanical characterization.

composite characteristics such as mechanical, structural, morphological, and rheological properties would be essential to obtain micro-mechanical modeling.

2. Material description and characterization methods

2.1. Material

Glass fiber-reinforced polypropylene (GF50-PP) composite with fiber weight fraction of 50% and density of 1.33 g/cm^3 was produced by the thermo-compression process. GF50-PP composite with a fiber length of about 4 cm was prepared as a randomly oriented GF50-PP plate (300 × 300 × 4 mm^3) to analyze its physicochemical, mechanical, and thermomechanical properties. The composition of the studied GF50-PP is presented in Table 1.

2.2. Sampling procedure according to the microstructural analysis

The samples used for pyrolysis analysis, ultrasonic measurements, and microscopic observations are shown in Fig. 1. Samples were cut into two or three parts through vertical lines according to Fig. 1. The weight and the volume of the samples were measured before performing pyrolysis measurements. Pyrolysis analysis was performed at the temperature of 450 °C for 5 h.

Fig. 2 presents the sampling area of the GF50-PP composite using ultrasonic results for mechanical characterizations.

2.3. Physicochemical characterizations

2.3.1. Microscopy observation

Microscopic observations were conducted by ZEISS Optical microscopy to observe glass fiber and porosity distribution in the polypropylene matrix from two directions: parallel and perpendicular to the Mold Flow Direction (MFD). The samples were picked off from different positions of the composite plate. Microscopic observations using Scanning Electronic Microscopy (HITACHI 4800 SEM) were utilized in order to study the composite microstructure and fiber orientation in the selected samples.

2.3.2. X-ray microtomography

X-ray microtomography permitted a three-dimensional imagining of GF50-PP composite. EasyTom nano setup, which is comprised of an X-Ray source, a rotating table, and an X-ray detector, was used to analyze the orientation of the fibers of the studied sample (1 × 1 × 3 cm^3) which was placed between the X-ray beam and the camera detector.

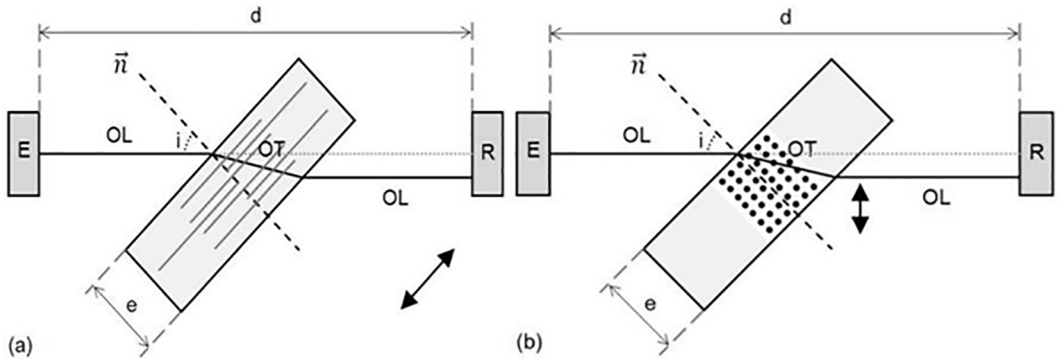

Fig. 3. Two limit cases for fiber orientation: (a) high V_{OT} and (b) low V_{OT}.

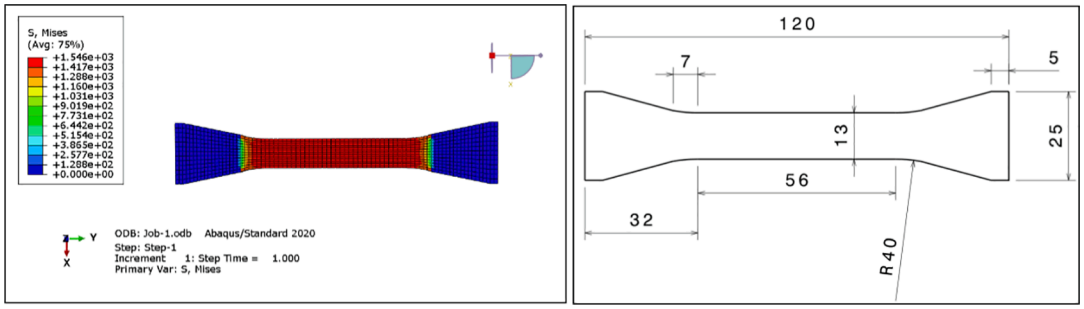

Fig. 4. Specimen geometry and dimensions applied for tensile test.

2.3.3. Ultrasonic measurement

The utilization of ultrasonic waves is a novel method proposed for characterizing the orientation distribution of the fibers in a composite. In this study, ultrasonic waves were used to present the orientation distribution of the fiber bundles in the GF50-PP composite. The ultrasonic measurements were carried out in immersion using an apparatus composed of two transmitting (E) and receiving (R) probes divided by a known and constant distance, d. The diameter of the probe was 10 mm. In order to generate a shear wave that propagates inside the material (in a direction determined by the Snell-Descarte law), the sample was located between two probes with an angle of about 45° from the incident ultrasonic wave. The ultrasonic shear stress was applied on the material in the plane defined by the incident wave (OL in Fig. 3) and the vector normal to the plane of the specimen ($\vec{n}$ in Fig. 3). The two limit cases, represented in Fig. 3, are the longitudinal orientation (Fig. 3 (a)), and transverse orientation of the fibers (Fig. 3 (b)). In the case of fibers' longitudinal orientation, the fibers lie within the ultrasonic shear stress plane, resulting in the maximum fiber section submitted to the shear stress. As a result, in case (a) with longitudinally oriented fibers, the maximum value of shear wave velocity, V_{OT}, will be measured. On the contrary, in case (b) with the transversely oriented fibers, the minimum fiber sheared section results in the minimum value of the shear wave velocity.

Accordingly, rotating the sample around the $\vec{n}$ axis from 0° to 360°, varies the value of V_{OT} in line with the orientation distribution of the fibers. In the strongly oriented samples, the V_{OT} curve becomes symmetric; however, in samples comprising of out-of-plane fiber orientations, the V_{OT} curve is non-symmetric. Conclusively, ultrasonic measurement is a practical and convenient method used for evaluating the distribution of fiber orientation using the evolution of shear wave velocity.

2.4. Thermomechanical properties: DMTA

Thermo-mechanical (DMTA) flexural tests were performed on a sample selected from the central position of the GF50-PP plate to indicate the main transition temperatures as well as loss, storage, and complex moduli of the GF50-PP composite using the "TA Instruments DMA Q800" instrument. The flexural test was carried out at a temperature range starting from −70 °C to 140 °C, with a heating rate of 2 °C/min, and a bending frequency of 1 Hz.

2.5. Mechanical characterizations

2.5.1. Quasi-static tensile test

The quasi-static tensile experiments were conducted with the INSTRON 5966 machine, using a 10 kN load cell and a displacement rate of 5 mm/min. For verifying the reproducibility of the results, at least five samples were carried out in a tensile test study for three fiber orientations of 0° (parallel to the mold flow direction (MFD)), 45°, and 90° (perpendicular to the MFD). To perform the mechanical tests, the geometry of the sample has been optimized using ABAQUS Explicit

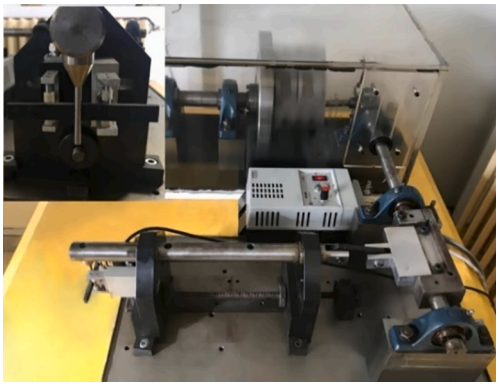

Fig. 5. The mechanical system of the three-point bending fatigue test apparatus.

according to the procedure presented in the previous works [29,45]. Several geometries have been analyzed. The increasing gage length and radius do not affect the stress concentration; however, the most important geometric factor is the distance between gage length and shoulders. Fig. 4 schematically illustrates the employed dimensions of the tensile and fatigue test samples.

2.5.2. Quasi-static loading–unloading tensile tests

Quasi-static loading–unloading tensile tests at the different maximum applied stresses were performed on INSTRON 5966 machine with a loading speed of 2 mm/min to estimate the macroscopic stiffness reduction during tension.

2.5.3. Tension-tension fatigue test

Tension-tension stress-controlled fatigue tests were performed at different applied maximum stress (σ_{max}) using an MTS 830 hydraulic fatigue machine. The minimum applied stress (σ_{min}) was equal to 10% of the maximum applied stress associated with the stress-ratio of $R_\sigma = 0.1$ and the mean stress level of 0.55 σ_{max}. The experimental procedure was performed at the frequency of 10 Hz and the temperature of 20 °C. The damage evolution was evaluated using measuring Young's modulus evolution. Fatigue experiments were carried out on samples cut from three different directions from the MFD (0°, 45°, and 90°).

2.5.4. Three-points bending fatigue test

Three-points bending fatigue tests were conducted at different applied maximum strains (ε_{max}) to determine the bending fatigue strength of the composite in a very high-cycle regime. The minimum applied strain (ε_{min}) was equal to 10% of the maximum applied strain, resulting in the chosen strain-ratio value of $R_\sigma = 0.1$ and the mean strain-level of 0.55 ε_{max}. The tests were performed at the frequency of 10 Hz and the temperature of 20 °C. Fig. 5 illustrates the mechanical system used for the three-point bending fatigue test of GF50-PP composite.

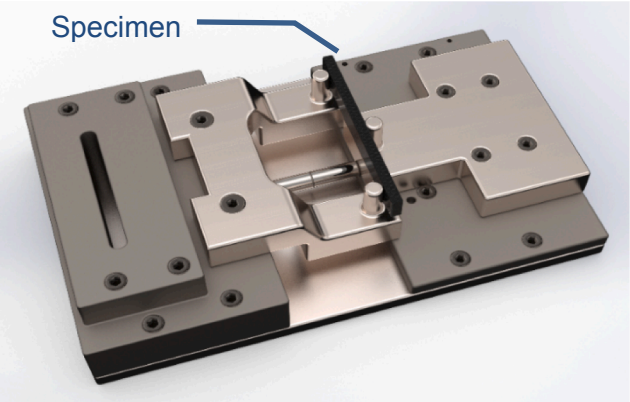

Fig. 6. The schematic of the micro-machine used for flexion test.

2.5.5. Damage analysis: in-situ three-point flexion test

In situ three-point flexion tests were performed by applying maximum travel of 20 mm at the rate of 0.5 mm/min to the center of the specimen (width: 5.2 mm and thickness: 1.9 mm) using a micro-machine (Fig. 6) with a span length of 28 mm, which was positioned inside a large SEM chamber (HITACHI 4800 SEM).

3. Experimental results and discussion

3.1. Microstructural observations

Fig. 7(a) represents the microscopic observations of composite's cross-sections in two directions of view: parallel and perpendicular to the MFD. The SEM images are taken from the two different directions, visually illustrate quite the same densities of different fibers' orientations, which indicates that there is no preferred fiber orientation, and the fibers are randomly oriented within the composite. The evolution of fiber orientation has been studied more precisely through ultrasonic measurements.

During the thermo-compression, the "multi-layer foam" is subjected to a flow allowing the mold to be filled. An X-ray microtomography observation (Fig. 7(b)) shows that the microstructure of the glass mat layer can be considered as an assembly of clusters linked together by entanglement at the location of the needling zones. The needling zones constitute "pits" in which the polymer can flow more easily, which can lead to disentanglement during creep under the effect of local pressure.

3.2. Microstructural analysis using ultrasonic measurement

The results of ultrasonic analysis collected from the approach described in the section 2.3.2, are shown in Fig. 8. The evolutions of the shear wave velocity for samples removed from different areas of the randomly-oriented composite plate present an almost circular polar diagram of velocity for the majority of samples, indicating that the orientation of fibers in the central area of the composite plate is quite homogeneous and there is no preferred orientation of fibers. However, the two samples indicated as numbers 1 and 24 located at the edges of the composite plate present a preferred fibers orientation of 330°, with a 30° deviation from the MFD. Overall, as it was shown in Fig. 7, the composite plate is composed of randomly oriented glass fibers with no preferred fiber orientation, especially at areas farther away from the edges, confirming the results of SEM observations.

The propagation velocity of the ultrasonic waves is dependent on the microstructure and mechanical properties of the material. The acoustical birefringence, coefficient K (%), is defined as:

$$K(\%) = 100\% \times (V_{OTmax} - V_{OTmin})/V_{OT\text{average}} \quad (1)$$

where V_{OT} is the velocity of the shear waves for a given relative orientation of the composite (see Fig. 3). This coefficient provides orientation intensity for comparing the distribution of fibers orientation in a way that high values of K suggest the predominant orientation of fibers. Moreover, in terms of the spatial distribution of the fibers, high values of density, tensile, and shear wave velocities demonstrate the presence of a large number of fibers at the test location. Table 2 presents the average values of K, V_{OT}, and V_{OL} for the 24 tested samples.

3.3. Pyrolysis analysis

The fiber mass fraction of the GF50-PP composite has been calculated by fiber separation using the pyrolysis process at 450 °C for 5 h. Table 3 demonstrates mass and volume fractions. The density of composite samples has been calculated using Archimedes' method, and porosity content has been estimated according to the glass fiber mass fraction and initial composite density.

The porosity content for different areas of GF50-PP composite after compression molding is about 0.86% at maximum value, which is inferior to 1%. This suggests that the produced composite with a specific fiber orientation can present a homogeneous behavior under loading.

3.4. Thermomechanical properties

To determine the main transition temperatures, the DMTA test was employed on a GF50-PP sample using a dual cantilever at a strain of 0.01%, frequency of 1 Hz, and temperature range of −70 °C to 140 °C. Fig. 9 shows the evolution of storage modulus and loss modulus as a function of temperature for this composite. GF50-PP shows a glass transition temperature lying between about 40 °C and 130 °C. Two temperatures corresponding to β-transition, T_β (at about 67.7 °C), and α-transition, T_α (at about 6.6 °C), are recognized. At T_β, a brittle-ductile transition for amorphous phase occurs, which is generally related to the mobility of the small segments of molecular chains near the surface of crystallites. This phenomenon is likely to happen due to the stiffening of chain segments between the amorphous phase and crystalline phase as well as *trans*-crystallization at the fiber–matrix interface. It is noticeable that the values of storage modulus are temperature-dependent. After T_β, the storage modulus starts to decrease significantly.

At −70 °C, the value of storage modulus is 6695 MPa, while at 20 °C this value is 5188 MPa, which represents a decrease of 22.5%. Although the storage modulus decreases with temperature rise due to the increase of macromolecular chain mobility, the GF50-PP composite remains rigid at 20 °C.

The correlation of data from the thermo-mechanical (DMTA) flexural test to linear data from the quasi-static mechanical test is achievable. As the α-transition is about 6.6 °C, it is important to analyze the quasi-static behavior of the composite at the two temperatures of −70 °C and 20 °C.

3.5. Quasi-static tensile test

Uniaxial quasi-static tensile tests at different temperatures and three fiber orientations of 0°, 45°, and 90° have been conducted in order to calculate the ultimate stress limit and the initial Young's modulus of the samples, as well as to estimate the macroscopic stiffness reduction as an indicator of the microscopic damage. For determining the uncertainty and repeatability of test results, at least three samples were investigated for each condition in terms of temperature and fiber orientation of the composite. For example, Fig. 10 demonstrates obtained tensile test results for fiber orientation of 45° and a temperature of 20 °C. It is noticeable that a homogeneous composite plate can be obtained after the compression molding process of GF50-PP composite, as shown in the ultrasonic results section. The latter also confirms the efficiency of the sampling procedure for mechanical tests. The obtained results from pyrolysis present that the porosity percentage of GF50-PP composite is highly acceptable.

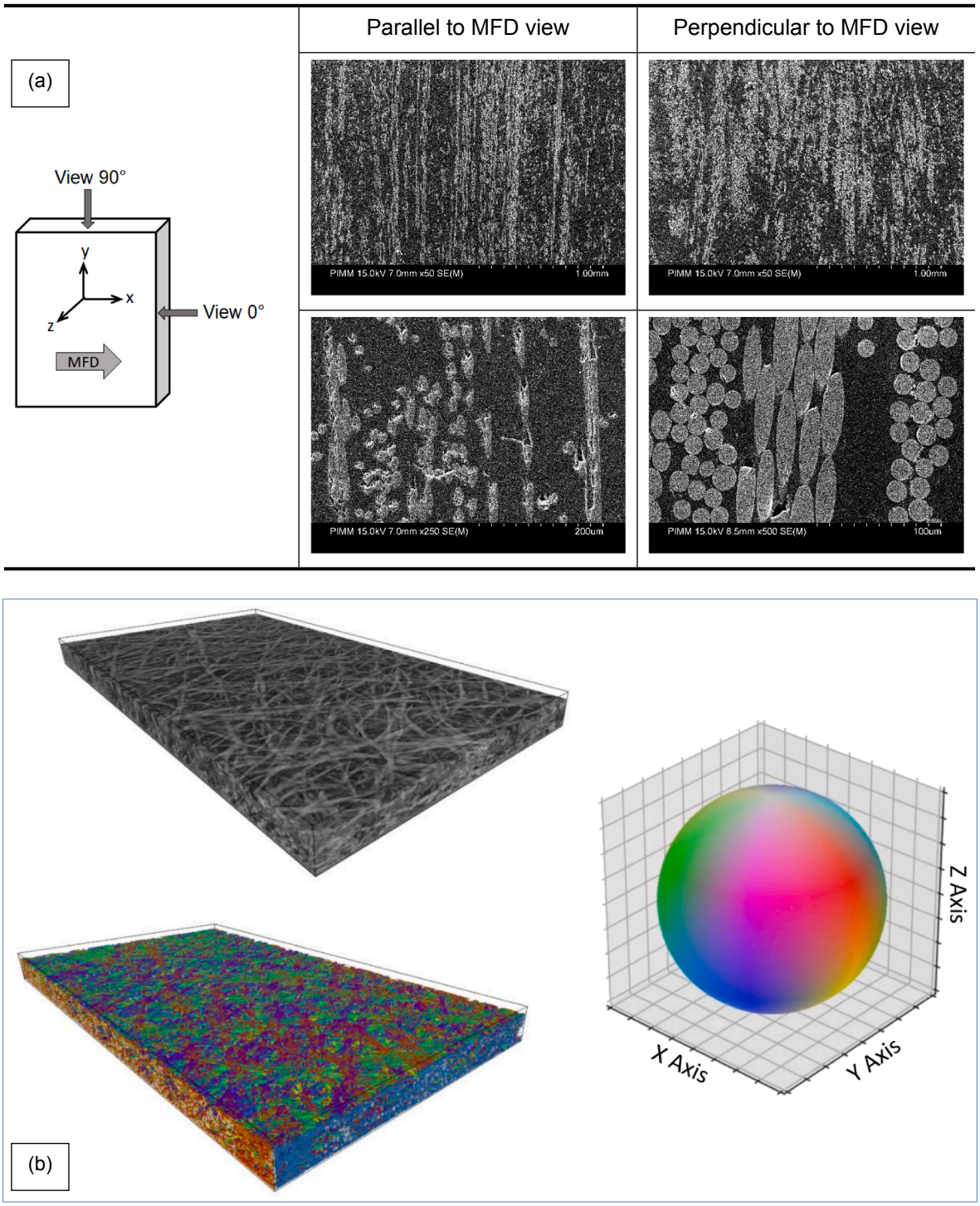

Fig. 7. Microstructure of GF50-PP composite: randomly oriented bundles of fibers, SEM micrographs (a) and X-ray microtomography (b).

3.5.1. Effect of temperature

The tensile behavior of polypropylene is highly sensitive to temperature as its glass transition temperature is about 6.6 °C. Different mechanical behaviors would be normally considerable at ambient temperature in comparison to cryogenic temperatures. However, the GF50-PP composite presents special tensile behavior at ambient temperature compared to cryogenic temperatures.

Fig. 11 shows the tensile results of GF50-PP composite at the temperatures of 20 °C and −70 °C for three fiber orientations of 0°, 45°, and 90°. From these results, it is noticeable that there is no difference in Young's modulus and failure strain under loading temperatures of 20 °C and −70 °C. By cooling the polymer down to the cryogenic temperatures, unequal coefficients of thermal expansion between the fibers and the matrix would cause significant internal stress that would eventually initiate the formation of microcracks in the polymer matrix [44]. The presence of microcracks is the main reason for the difference in the curves illustrated in Fig. 11. Another aspect that should be noticed is fiber orientation. By changing fiber orientation from 0° to 45° and 90°, the difference between tensile behavior of GF50-PP under loading temperatures of 20 °C and −70 °C decreases. This difference is highlighted in the tensile curves of Fig. 11.

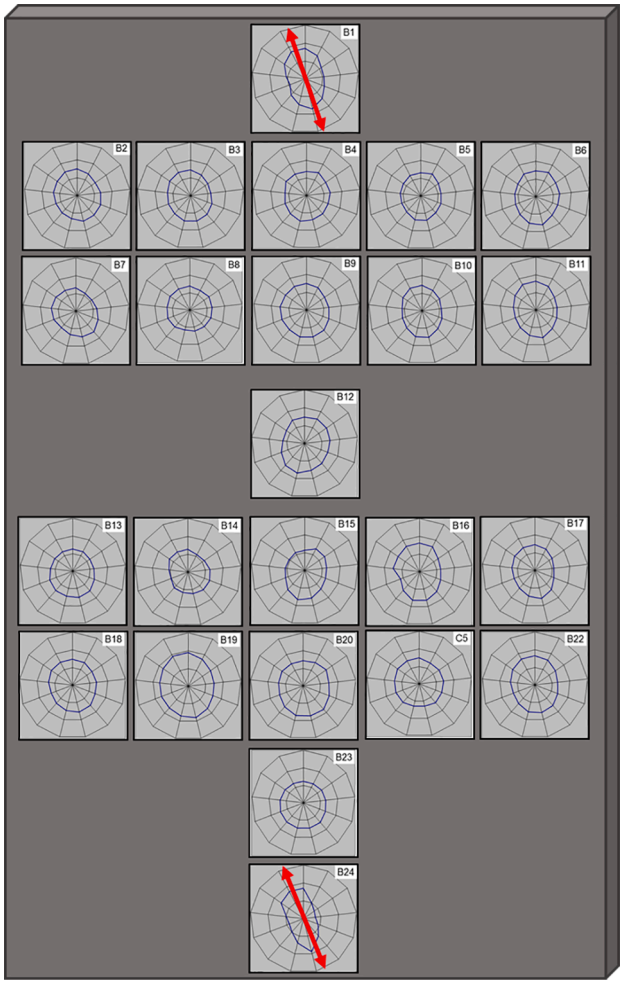

Fig. 8. Ultrasonic results of the GF50-PP composite plate.

Table 2
The average values of K, V_{OT}, and V_{OL}, obtained from ultrasonic measurements.

Parameter	Value
K (%)	2.8
V_{OT} (m/s)	1536
V_{OL} (m/s)	2542

Table 3
GF50-PP sample composition.

Code	Composite	Glass fiber		PP		Porosity
	ρ (g/cm^3)	Wt.%	Vol.%	Wt.%	Vol.%	Vol.%
1	1.33	48.13%	24.83%	51.87%	75.04%	0.13%
3	1.39	53.22%	28.61%	46.78%	70.52%	0.86%
5	1.39	52.96%	28.49%	47.04%	70.96%	0.54%
7	1.44	56.52%	31.59%	43.48%	68.14%	0.26%
9	1.37	51.87%	27.52%	48.13%	71.62%	0.85%
11	1.38	52.14%	27.89%	47.86%	71.79%	0.32%
12	1.36	50.62%	26.61%	49.38%	72.78%	0.61%
14	1.38	52.68%	28.22%	47.32%	71.08%	0.70%
16	1.38	51.76%	27.61%	48.24%	72.15%	0.25%
18	1.38	52.05%	27.82%	47.95%	71.87%	0.31%
20	1.39	52.36%	28.13%	47.64%	71.77%	0.10%
22	1.37	51.31%	27.17%	48.69%	72.30%	0.54%
23	1.37	51.20%	27.17%	48.80%	72.61%	0.22%
24	1.32	47.41%	24.28%	52.59%	75.51%	0.22%

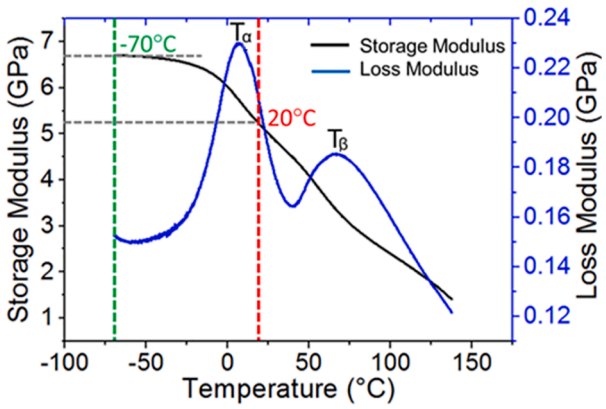

Fig. 9. DMTA diagram showing the types of transitions for GF50-PP composite.

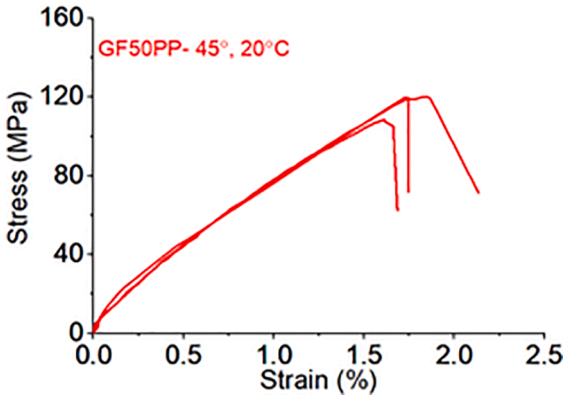

Fig. 10. The quasi-static tensile test results of GF50-PP samples with fiber orientation of 45° at 20 °C.

3.5.2. *Effect of fiber orientation*

Fig. 12 illustrates the tensile properties of the GF50-PP composite samples at ambient (20 °C) and cryogenic (-70 °C) temperatures for samples with different fiber orientations.

During thermo-compression molding of fiber-reinforced composites, the fibers are exposed to a variety of complex effects leading to fiber orientation, fiber–matrix separation, length grading, and fiber distribution, which altogether affect the mechanical properties of the composite. Consequently, the fiber-reinforced composite products may represent a variety of mechanical properties initiated from the design process [35]. In addition, generally, for most materials, the tensile test results at cryogenic temperatures lead to different breakage regimes and lower toughness. However, these aspects are not significant in the case of the GF50-PP composite. Tensile test results demonstrate that at loading temperature of 20 °C, the maximum stress of samples with three fiber orientations of 0°, 45°, and 90° are almost similar. The same phenomenon can be observed at a loading temperature of −70 °C, while in this low temperature the values of maximum stress are higher than those at 20 °C. The results also confirm that there is no effect of fiber orientation on the tensile results for the two loading temperatures of 20 °C and −70 °C. Fig. 12 also presents that there is no significant difference between the values of failure strain at loading temperatures of 20 °C and −70 °C. This behavior is related to the special microstructure of this composite during and after the processing steps. It is noticeable that during the thermo-compression process, the “multi-layer foam” is subjected to a flow allowing the mold to be filled. Microscopic observation showed that the microstructure of the glass mat layer can be considered as an assembly of clusters linked together by entanglement at the location of the needling zones. The latter constitute “pits” in which the polymer can flow more easily, probably causing disentanglement

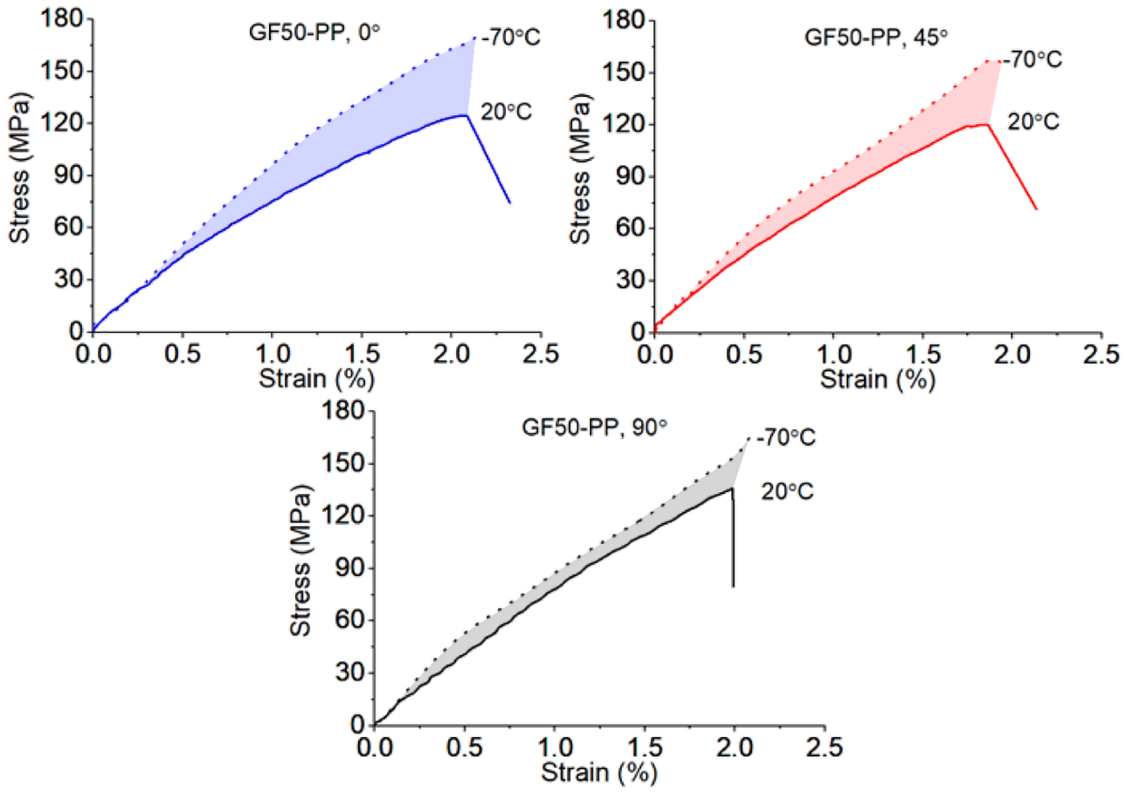

Fig. 11. The quasi-static tensile test results of GF50-PP sample at the temperatures of 20 °C and −70 °C for three fiber orientations of 0°,45°, and 90°.

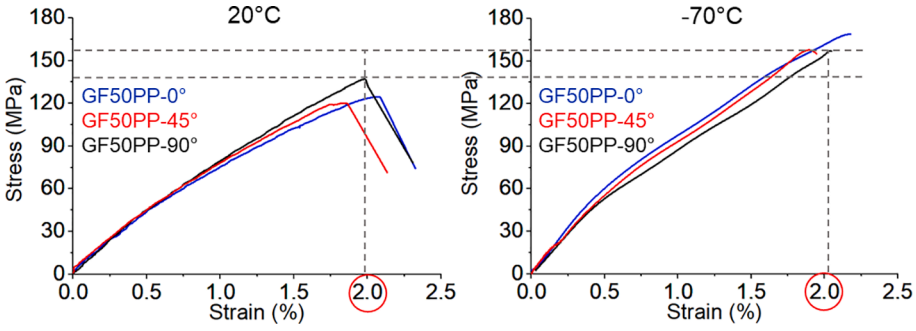

Fig. 12. Tensile curves for samples of different fiber orientations at temperatures of 20 °C and −70 °C.

Table 4
Tensile properties of GF50-PP.

Sample		E GPa	σ_y MPa	ε_y %	σ_{max} MPa	ε_{max} %
−70 °C	0°	12.8	68.6	0.37	168.9	2.17%
	45°	12.4	63.9	0.46	158.3	1.85%
	90°	12.5	65.3	0.33	156.4	2.06%
20 °C	0°	8.1	35.9	0.53	124.6	2.07%
	45°	8.2	37.3	0.55	120.2	1.83%
	90°	8.2	34.5	0.54	137.0	1.98%

during creep under the effect of local pressure.

Table 4 describes the main mechanical characteristics, indicating their averages and deviations. According to the table, no anisotropy induced by the preferred orientation of the fibers is observable.

3.6. Macroscopic damage and apparent plasticity evolution during loading–unloading tests

Fig. 13 presents quasi-static loading–unloading response and monotonic stress–strain curves for the GF50-PP composite with the three configurations of 0°, 45°, and 90° at 20 °C.

The related diagrams display that there is no significant difference between monotonic and cyclic envelopes for all composites with different fiber orientations, which confirms that there is no considerable change in the failure behavior of GF50-PP composite tested by either loading–unloading or tensile loading tests. Moreover, there is no obvious dependency between the fiber orientation of GF50-PP samples and their plasticity evolution during the loading–unloading test.

Fig. 14 presents the loading–unloading response and the monotonic stress–strain curves of GF50-PP composite for the three fiber orientations of 0°, 45°, and 90° at −70 °C. Similar to the loading–unloading tests performed at 20 °C, there is no significant difference between the monotonic and the cyclic envelopes for the composites with the fiber orientations of 0° and 90°. However, for the composite with fibers

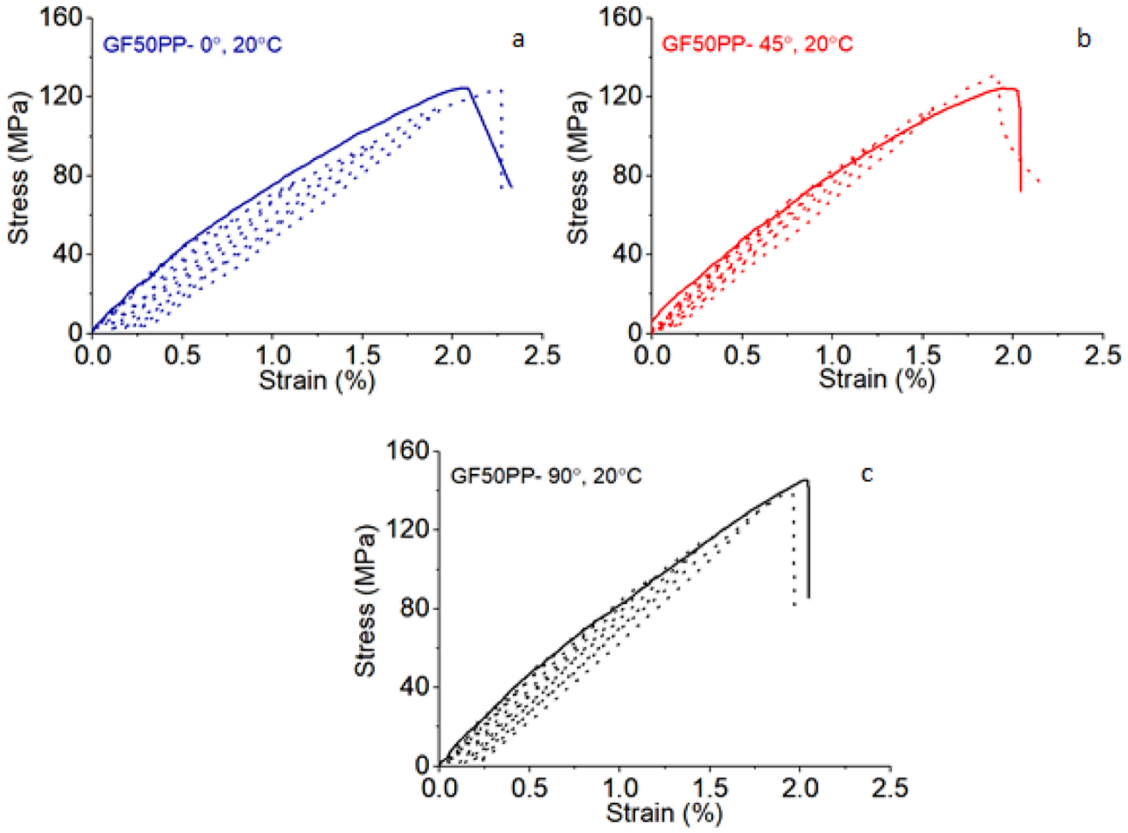

Fig. 13. Loading-unloading and monotonic stress–strain curves for GF50-PP composites including fibers oriented at 0° (a), 45° (b), and 90° (c) to the MFD at 20 °C.

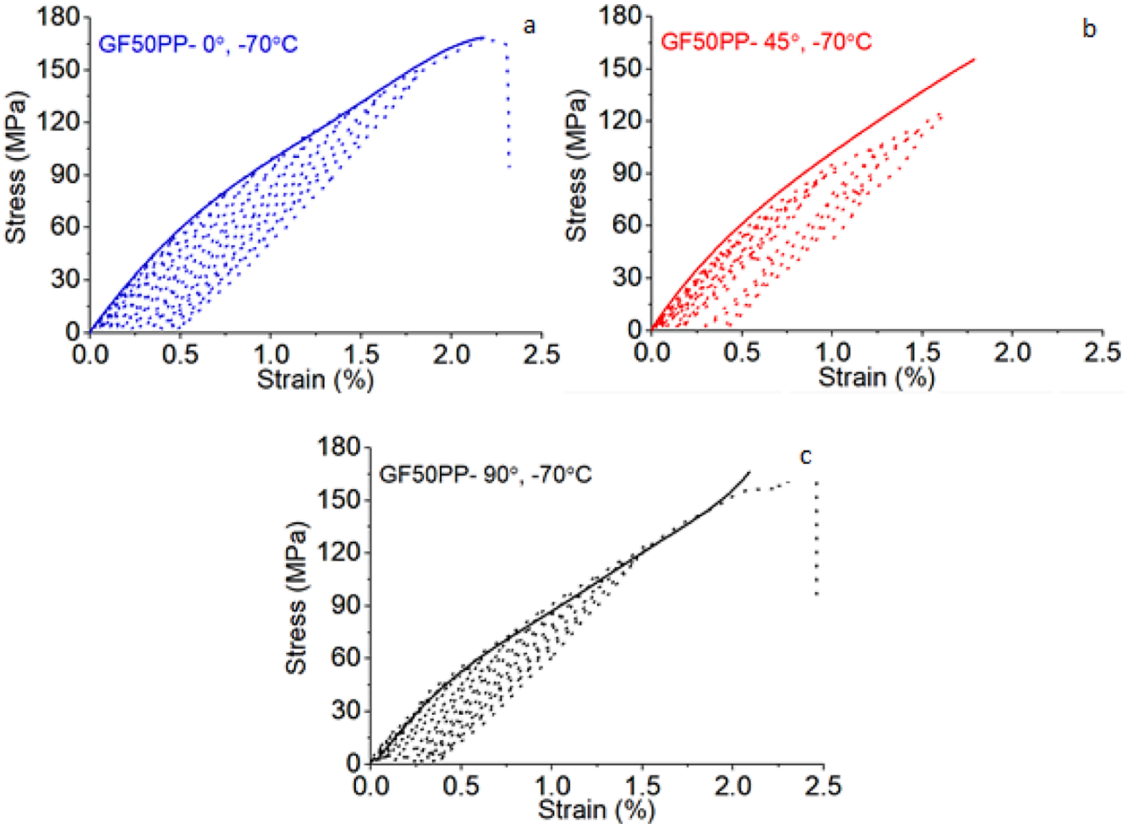

Fig. 14. Loading-unloading and monotonic stress–strain curves for GF50-PP composites including fibers oriented at 0° (a), 45° (b), and 90° (c) to the MFD at −70 °C.

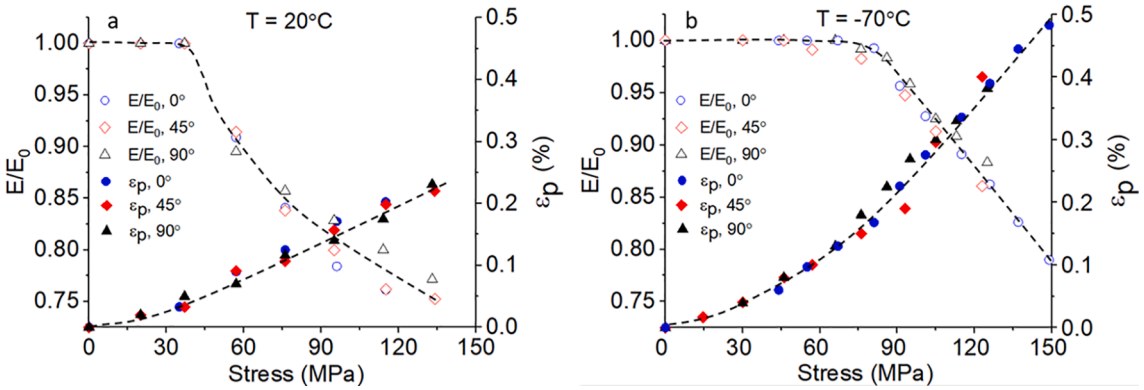

Fig. 15. Damage and residual strain (apparent plastic strain) evolution during loading–unloading quasi-static tests for 0°, 45°, and 90° fiber orientations of GF50-PP composite at 20 °C and −70 °C.

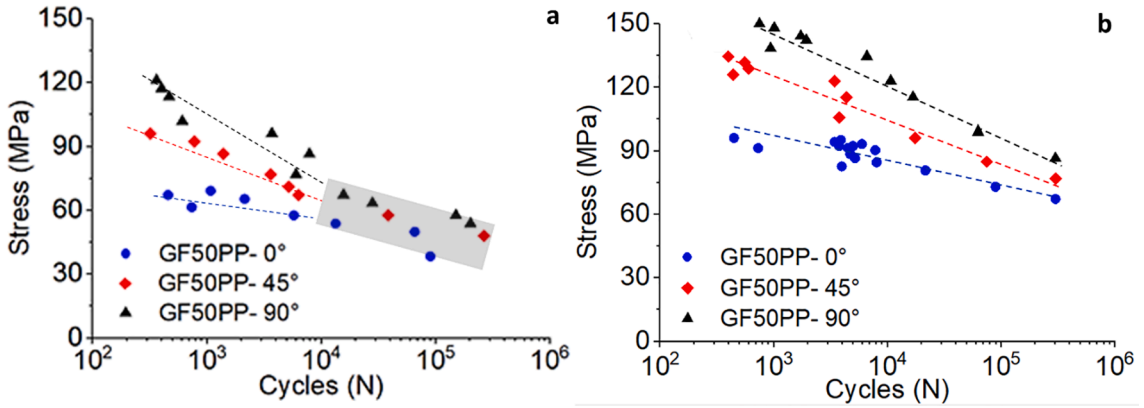

Fig. 16. S-N curves of stress-controlled tension–tension fatigue tests at 10 Hz: (a) 20 °C and (b) −70 °C.

orientated at 45° to the MFD, the difference between the two monotonic and the cyclic envelopes is quite noticeable.

Fig. 15 presents damage and residual strain (apparent plastic strain) evolution during quasi-static loading–unloading tests for 0°, 45° and 90° fiber orientations of GF50-PP composite at 20 °C and −70 °C. For the three different fiber orientations of composite, the plasticity threshold is lower than the damage threshold, resulting in the presence of two deformation stages involving matrix inelasticity and coupling damage to plasticity. It is noticeable that by reducing the temperature from 20 °C to −70 °C, the plasticity threshold doesn't change considerably, and the plastic strain at the threshold remains at about 15 MPa. On the contrary, the damage threshold reaches higher values from about 37 MPa to 65 MPa by decreasing the temperature from 20 °C to −70 °C, indicating that damage evolution, unlike plasticity, is dependent on temperature. It is also evident that the curves related to all the three fiber orientations in terms of damage or plasticity evolution present quite the same evolution. This means that there is no relation between the macroscopic loss of stiffness or the increment of plastic strain and fiber orientation of the composite.

3.7. Tension-tension fatigue test: Effect of fiber orientation and temperature

Fig. 16 provides a comparison between the fatigue behaviors of specimens with different fiber orientations in tension–tension loading mode (stress-controlled), at (a) ambient temperature and (b) cryogenic temperature. In ambient temperature, all the curves present bi-linear behavior related to low and high loading amplitudes, while cryogenic curves demonstrate almost linear behavior in the loading amplitude range. For all three fiber orientations, by increasing loading amplitude, fatigue lifetime decreases.

According to the diagram of ambient temperature, Fig. 16(a), two different sections of behavior are considerable: (1) high amplitude fatigue, in which a significant difference in behavior between composites with different fiber orientations is detectable, and (2) low amplitude fatigue, where all samples demonstrate almost the same behavior. Moreover, the slope of the curves (the kinetic) related to the first zone (high amplitude fatigue) is higher for the fatigue tests of GF50-PP-0° compared to the others. Consequently, one can note that different damage mechanisms are probably engaged in the fatigue behavior depending on the applied stress level.

Nevertheless, the cryogenic temperature curves demonstrate almost uniform linear behavior, but still sensitive to the fibers' orientation. According to this, a significant difference in the results of composite samples with varied fiber orientations is observable. For instance, for a stress amplitude of approximately 80 MPa, the samples with the fiber orientation of 90° (perpendicular to the MFD), present a lifetime about a hundred times (up to 0.5×10^6 cycles) as higher as the lifetime of 0.5×10^4 cycles for the samples with the fiber orientation of 0° (parallel to the MFD).

It can be assumed that different fiber orientations would lead to different decohesion sensitivity in the fiber–matrix interface. Moreover, the anisotropic mechanical behavior resulted from fiber addition, makes the composites sensitive to the loading mode, despite their relatively high strength under normal tension stress.

Furthermore, some mechanisms including probable local self-heating can be suggested as a participating factor in the fatigue tests performed at ambient temperature. However, such mechanisms would

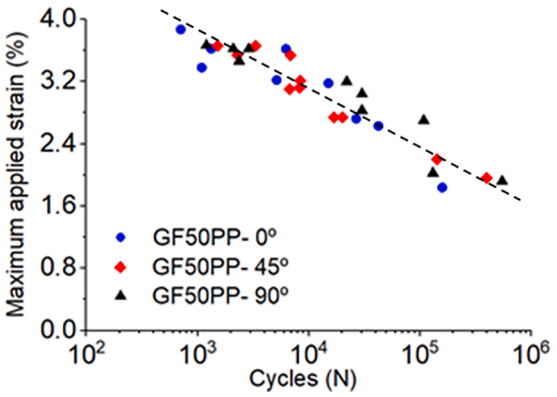

Fig. 17. S-N curves of strain-controlled three-point bending fatigue tests at 10 Hz.

not be feasible under cryogenic conditions.

3.8. Three-point bending fatigue test: effect of fiber orientation

Fig. 17 shows the 10 Hz S-N curves of the three-point bending fatigue test for samples under a loading temperature of 20 °C. Unlike tensile-tensile fatigue results, the fatigue lifetime for three fiber orientations of 0°, 45°, and 90° are similar. One can notice that strain-controlled three-point bending fatigue tests have been applied and the results confirm there is no fiber orientation dependency for GF50-PP composite. In addition, by increasing the applied strain, the fatigue lifetime decreases. The linear fitting curve in the logarithmic scale has been presented in Fig. 17.

3.9. Macroscopic damage analysis in fatigue

The evolution of the relative stiffness, E/E_0, and normalized stress of the GF50-PP composite with an elasto-plastic damage behavior, can be used as a damage indicator.

3.9.1. Tension-tension fatigue test at 20 °C

Loading conditions including frequency and amplitude can induce self-heating as a result of the fatigue behavior, which can affect the viscous behavior of the material. Applying high frequency or high applied stress increases the self-heating and leads to "induced thermal fatigue'' (ITF). Lower frequencies are often associated with a fatigue behavior called "mechanical fatigue'' (MF) induced by microscopic-scale damage mechanisms such as fiber–matrix interface debonding, micro-cracking of the matrix, and pseudo-delamination between the fibers [29]. The fatigue behavior of GF50-PP composite with three different fiber orientations for five different loading conditions is analyzed in this section.

Fig. 18 illustrates the evolution of the relative Young's modulus during tension–tension fatigue tests with different maximum applied stresses for the three studied fiber orientations. Considering continuum damage mechanics, the reduction of dynamic stiffness can be used as a damage indicator during fatigue.

At low cycles (up to about 100, 200, and 1000 cycles for fiber orientations of 0°, 45°, and 90°, respectively) the reduction of dynamic stiffness obeys the same trend under different maximum applied stresses. However, at higher cycles, the figures for the relative Young's modulus tend to present different evolutions. One can note that before the failure, two slopes of the stiffness reduction (P_{ITF} and P_{MF}) could be assigned to each curve. P_{ITF} is the rate of stiffness reduction during the predominant ITF stage and P_{MF} is the rate of stiffness reduction during

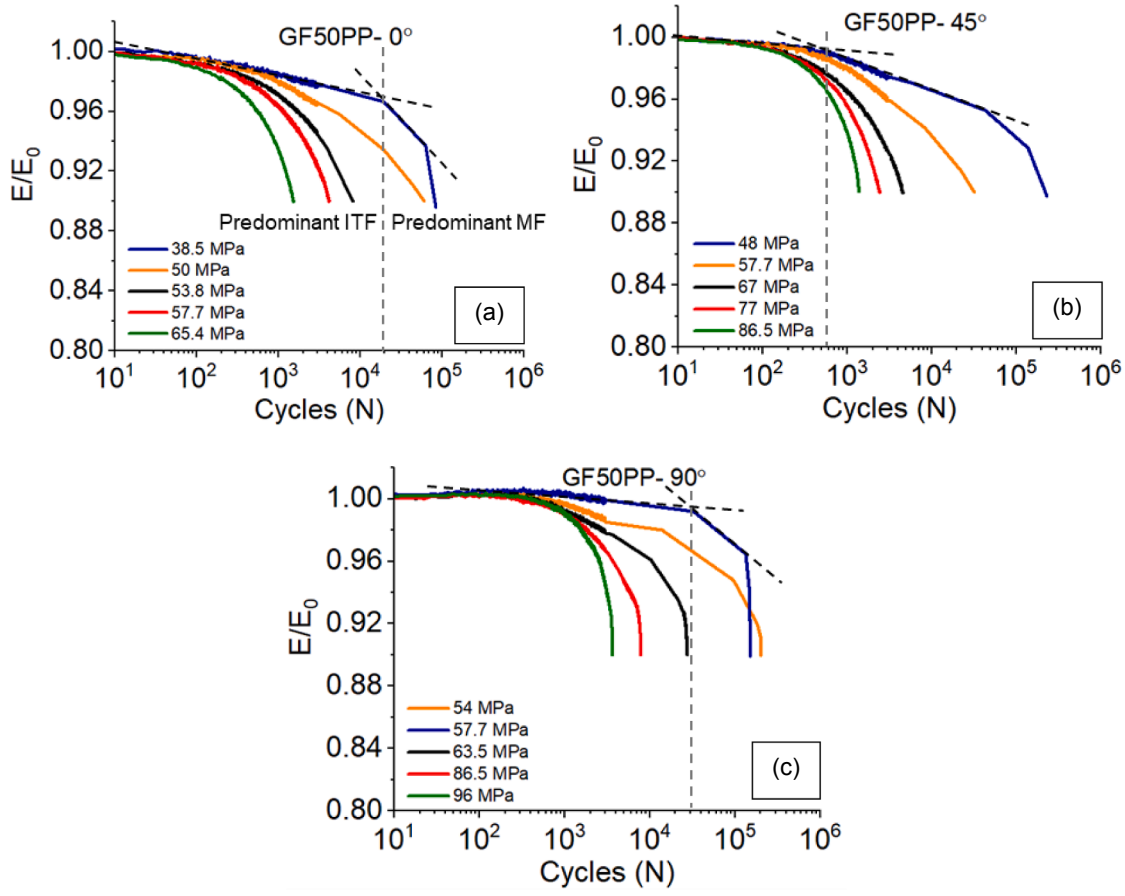

Fig. 18. Evolution of the relative Young's modulus during fatigue test at 10 Hz for three different fiber orientations in GF50-PP composite.

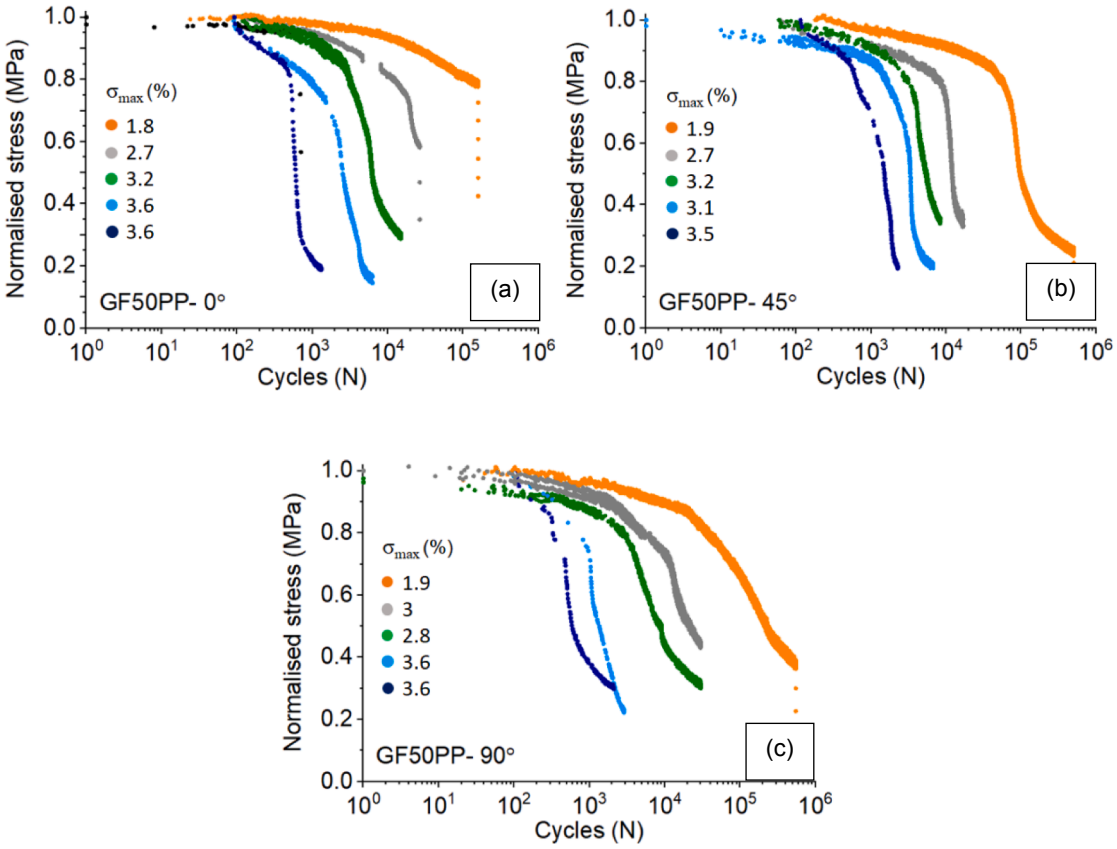

Fig. 19. Normalized stress curves versus cycle at a frequency of 10 Hz for three different fiber orientations of GF50-PP composite.

the predominant MF stage. By increasing the applied maximum stress in all three configurations, the transition point between the two stages moves to lower cycle numbers and mechanical fatigue becomes the main reason for failure. This indicates that by increasing the maximum applied stress, the fatigue lifetime decreases to lower numbers of cycles.

3.9.2. Three-point bending fatigue test at 20 °C

Normalized stress curves versus the number of cycles obtained from three-point bending fatigue tests at the frequency of 10 Hz with different ultimate stress values (amplitudes) for the three studied fiber orientations are shown in Fig. 19.

Two distinguished zones with different slopes of normalized stress reduction associated with the high and low cycles are identified for each curve. As it has been shown in Fig. 19, high loading amplitudes lead to lower fatigue life in all samples, regardless of their fiber orientation. For example, for applied stress equal to 0.8 σ_{max} for the sample with the fiber orientation of 0°, fatigue life decreases from about 2×10^5 to 10^3 by varying the maximum applied stress from 1.8 to 3.6. This difference even becomes more significant at lower values of the applied stress. Moreover, the reduction rate of the normalized stress increases with the increase of applied maximum stress.

3.9.3. Comparison of mechanical behavior in fatigue: tension–tension and 3-point bending

Fig. 20(a) represents the evolutions of relative Young's modulus during fatigue tests at 20 °C for three different fiber orientations of GF50-PP composite under the applied stress of 57.7 MPa. The related curves suggest that the trends of relative Young's modulus evolution are not the same for the three fiber orientations of the composite. In this case, the fiber orientations of 90° and 0° present the highest and the lowest fatigue lifetime, respectively.

Fig. 20(b) illustrates the evolutions of relative Young's modulus during fatigue tests at −70 °C for three different fiber orientations of GF50-PP composite under the applied stress of 96 MPa. The related curves suggest that the trends of relative Young's modulus evolution (slope of damage evolution) are the same for the three fiber orientations of the composite just before failure.

Fig. 20(c) shows the normalized stress curves versus cycle at a frequency of 10 Hz for three different fiber orientations of GF50-PP composite at the maximum applied stress of 3.2 %. Similar to the evolution of relative Young's modulus, the fiber orientations of 90° and 0° present the highest and the lowest fatigue life, respectively, under the maximum applied stress of 3.2 %. One can note that the same slope of damage evolution can be observed for the two stages of fatigue (Fig. 20(c)).

3.10. Multi-scale damage analysis: in-situ bending test

To understand the physical origin of the damage evolution and identify the corresponding damage mechanisms in GF50-PP composite, experimental investigations at the microscopic scale have been performed. Identifying the influence of the microstructure on damage mechanisms occurring at the local scale was carried out using a three-points quasi-static (0.5 mm/min) bending test performed on composite samples with three different fiber orientations. Fig. 21 illustrates the evolutions of the damage under the in-situ bending test for the three studied orientations. The results suggest that the values of ultimate displacement in 45° and 90° orientations are quite the same. However, in the sample with the orientation of 0°, the maximum force reaches higher values to around 650 N compared with the other two samples with lower ultimate displacements.

For each composite with different fiber orientations, macroscopic observations of the samples obtained at the beginning of the fiber–matrix interface debonding and at the ultimate stress corresponding to pseudo-delamination are presented by arrows. SEM images of failed

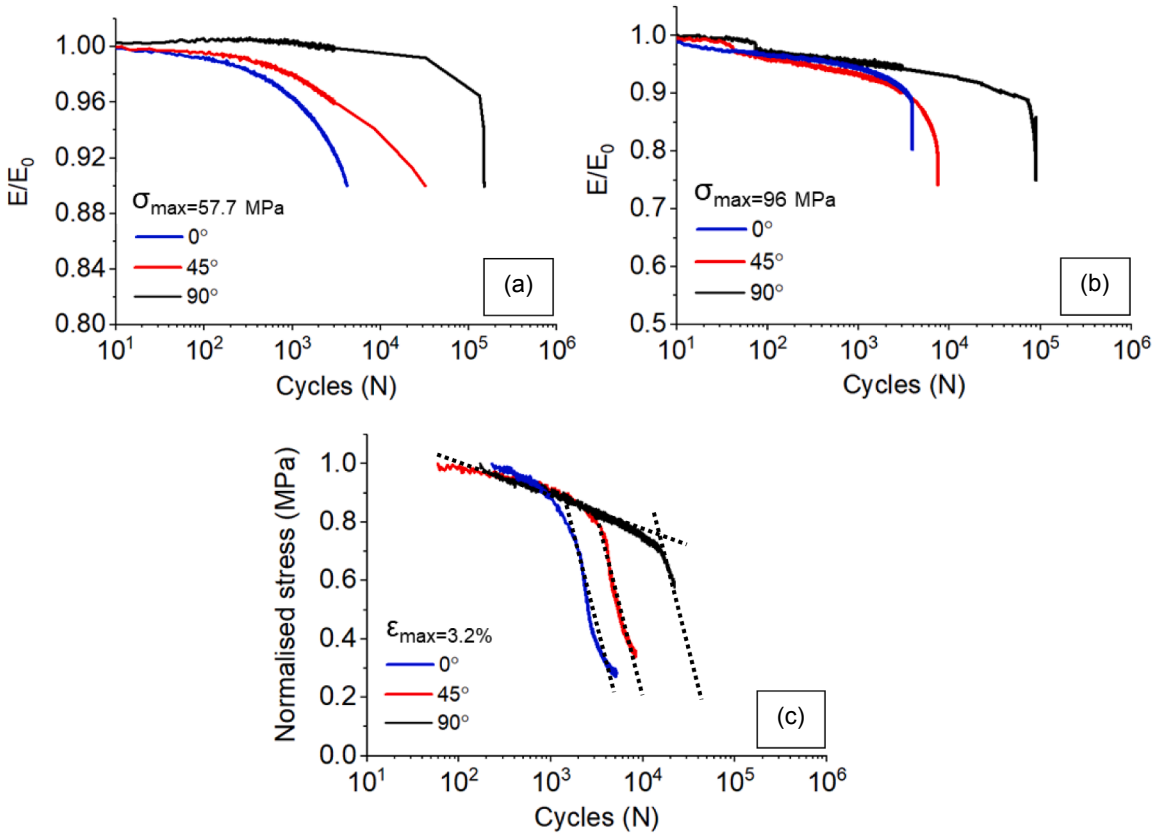

Fig. 20. Evolutions of the relative Young's modulus during fatigue tests at 10 Hz for three different fiber orientations of GF50-PP composite under the applied temperature of 20 °C (a), −70 °C (b); and normalized stress curves versus cycle at a frequency of 10 Hz for three different fiber orientations of GF50-PP composite under the maximum applied stress of 3.2 % (c).

samples are also included in the pictures. The presence of both pseudo-delamination between fibers and transversal micro-cracks appeared due to the coalescence of interface failure between adjacent fibers is noticeable in all three types of samples. For all the composite samples, debonding at the fiber–matrix interface and pseudo-delamination are the main mechanisms of damage. Consequently, the thresholds of fiber–matrix interface damage and delamination are not dependent on the fiber orientation of the randomly oriented GF50-PP composite.

Based on the several studies of Sun et al. [40–43,46], the material damage due to fatigue is dependent on the collective evolution of numerous internal cracks, especially in the regime of short-crack. Consequently, the damage in the multi-scale fatigue model involves the collective effect of all current cracks. The various short cracks in micro-scale cause overall deterioration of the composite in macro-scale.

4. Conclusion

Fiber-reinforced polypropylene composite (GF50-PP) composed of long glass fibers (4 cm, fiber weight fraction: 50%), produced by the thermo-compression method was investigated in terms of mechanical properties and multi-scale damage analysis. The SEM analysis performed on two different directions of samples presented the randomly oriented fiber orientation of the composite, which was further confirmed by ultrasonic results. The porosity content of the samples cut from different areas of GF50-PP composite was all beneath 1%, suggesting that the composite is homogeneous.

Tensile test results of the GF50-PP composite illustrated no difference in failure strain under loading temperatures of 20 °C and −70 °C. Moreover, by altering the fiber orientation from 0° to 45°, and 90°, the difference between tensile behavior of GF50-PP under loading temperatures of 20 °C and −70 °C decreased. Furthermore, at loading temperatures of both 20 °C and −70 °C, the maximum stress of samples with different fiber orientations are almost similar, while at −70 °C the values of maximum stress are higher than those at 20 °C. The tension–tension fatigue behavior analysis presented two different behaviors including high amplitude fatigue, and low amplitude fatigue. These results suggested the presence of different damage mechanisms engaged in the fatigue behavior depending on the applied stress level. Unlike tension–tension fatigue results, the fatigue life for three fiber orientations of 0°, 45°, and 90° are similar in 3-point bending fatigue tests. The results of damage analysis through monotonic loading presented that for the three different fiber orientations of composites, the plasticity threshold is lower than the damage threshold. By decreasing the temperature from 20 °C to −70 °C, the plasticity threshold didn't change notably; however, the damage threshold reached higher values. The results of multi-scale damage analysis through the in-situ bending test illustrated that the values of ultimate displacement in 45° and 90° orientations are quite identical. Macroscopic observations of the samples exhibited fiber–matrix interface debonding and pseudo-delamination at the beginning and the ultimate stress stage of the bending test, respectively.

Authors' contributions

Mohammadali Shirinbayan, Abbas Tcharkhtchi, Joseph Fitoussi: construct the idea. Mohammadali Shirinbayan, Mojdeh Rezaei-khamseh, Mohammad Hossein Nikooharf, Abbas Tcharkhtchi, Joseph Fitoussi: analyzed results, draft manuscript preparation, and wrote the paper. Mohammadali Shirinbayan, Mojdeh Rezaei-khamseh, Mohammad Hossein Nikooharf: corrected the English and the paper format.

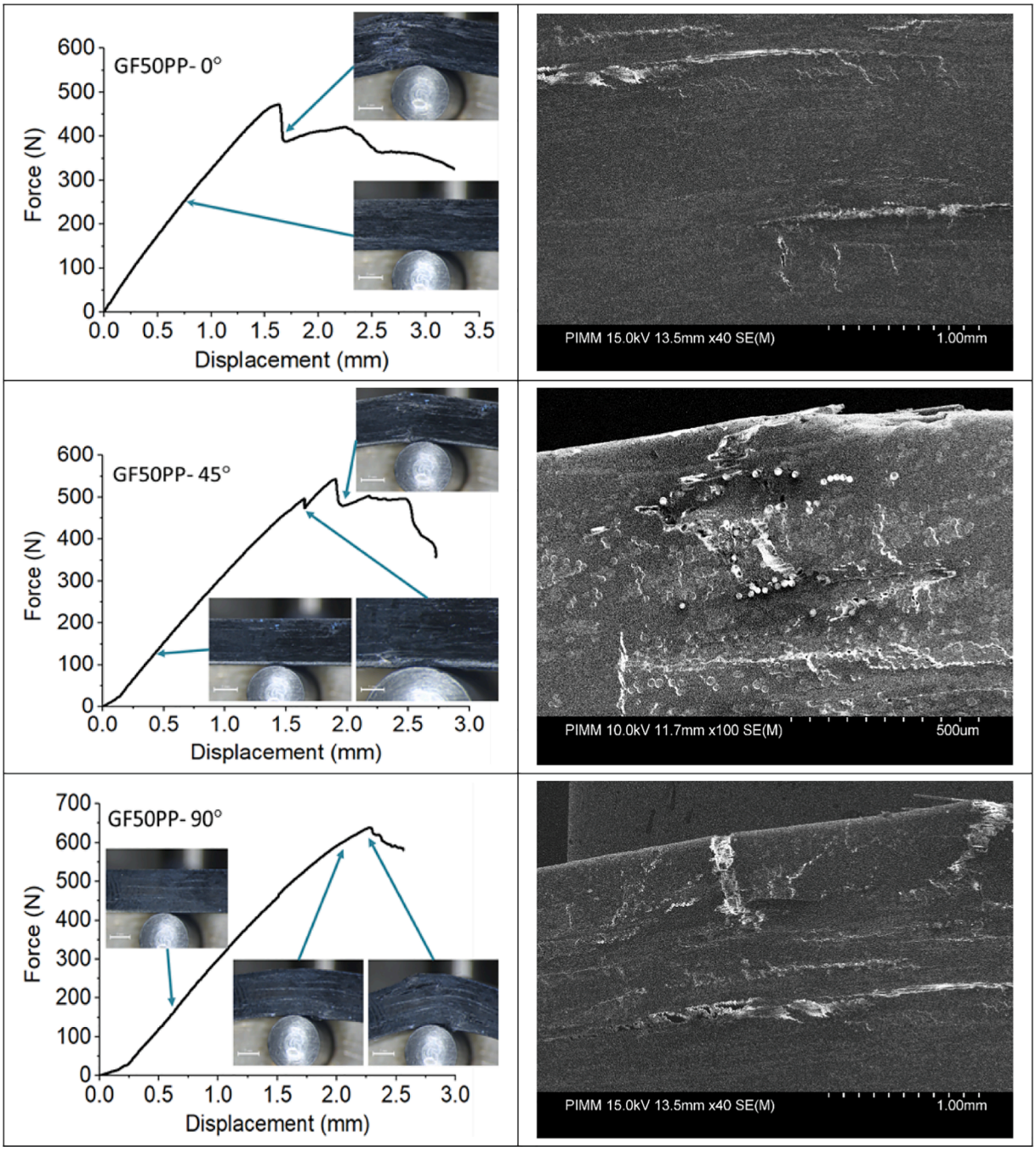

Fig. 21. Evolution of the damage under bending test for three studied fiber orientations of GF50-PP composite together with microscopic failure images.

Availability of data and materials

The authors declare that the data and the materials of this study are available within the article.

Declarations

Consent to participate: Not applicable.
Consent to publish: Not applicable.

Declaration of Competing Interest

The authors declare that they have no known competing financial interests or personal relationships that could have appeared to influence the work reported in this paper.

References

[1] Crema L, Sorgato M, Zanini F, Carmignato S, Lucchetta G. Experimental analysis of mechanical properties and microstructure of long glass fiber reinforced polypropylene processed by rapid heat cycle injection molding. Compos A Appl Sci Manuf 2018;107:366–73.
[2] Bazli L, et al. Application of composite conducting polymers for improving the corrosion behavior of various substrates: a review. J Comp Compd 2020;2(5):pp. 12/23.
[3] Abuchenari A, et al. A review on development and application of self-healing thermal barrier composite coatings. J Comp Compd 2020;2(4):pp. 09/30.
[4] Huang L, Wu Q, Wang Q, Wolcott M. Interfacial crystals morphology modification in cellulose fiber/polypropylene composite by mechanochemical method. Compos A Appl Sci Manuf 2020;130:105765.

[5] Gómez-Monterde J, Sánchez-Soto M, Maspoch ML. Microcellular PP/GF composites: morphological, mechanical and fracture characterization. Compos A Appl Sci Manuf 2018;104:1–13.
[6] Díez-Pascual AM, Naffakh M. Polypropylene/glass fiber hierarchical composites incorporating inorganic fullerene-like nanoparticles for advanced technological applications. ACS Appl Mater Interfaces 2013;5(19):9691–700.
[7] Kossentini Kallel T, Taktak R, Guermazi N, Mnif N. Mechanical and structural properties of glass fiber-reinforced polypropylene (PPGF) composites. Polym Compos 2018;39(10):3497–508.
[8] Gu S, Liu H, Li X, Mercier C, Li Y. Interfacial designing of PP/GF composites by binary incorporation of MAH-g-PP and lithium bis (trifloromethanesulfonyl) imide: towards high strength composites with excellent antistatic performance. Compos Sci Technol 2018;156:247–53.
[9] Kim D-H, Kang S-Y, Kim H-J, Kim H-S. Strain rate dependent mechanical behavior of glass fiber reinforced polypropylene composites and its effect on the performance of automotive bumper beam structure. Compos B Eng 2019;166:483–96.
[10] Kiss P, Stadlbauer W, Burgstaller C, Archodoulaki V-M. Development of high-performance glass fibre-polypropylene composite laminates: effect of fibre sizing type and coupling agent concentration on mechanical properties. Compos A Appl Sci Manuf 2020;138:106056.
[11] Yudhanto A, et al. Monotonic and cyclic responses of impact polypropylene and continuous glass fiber-reinforced impact polypropylene composites at different strain rates. Polym Test 2016;51:93–100.
[12] Arikan V, Sayman O. Comparative study on repeated impact response of E-glass fiber reinforced polypropylene & epoxy matrix composites. Compos B Eng 2015;83:1–6.
[13] Chen H, Wang J, Ni A, Ding A, Sun Z, Han X. Effect of novel intumescent flame retardant on mechanical and flame retardant properties of continuous glass fibre reinforced polypropylene composites. Compos Struct 2018;203:894–902.
[14] Duan S, Zhang Z, Wei K, Wang F, Han X. Theoretical study and physical tests of circular hole-edge stress concentration in long glass fiber reinforced polypropylene composite. Compos Struct 2020;236:111884.
[15] Bazli L, et al. Electrical properties of polymer blend composites based on Silicone rubber/EPDM/clay for high voltage insulators. J Comp Compd 2021;3(6):pp. 03/28.
[16] Kim D-J, Yu M-H, Lim J, Nam B, Kim H-S. Prediction of the mechanical behavior of fiber-reinforced composite structure considering its shear angle distribution generated during thermo-compression molding process. Compos Struct 2019;220:441–50.
[17] Hoang TQT, Touchard F. Non-woven flax fibre reinforced polypropylene: Static and low velocity impact behaviour. Polym Polym Compos 2013;21(5):287–98.
[18] Kuhn C. Analysis and Prediction of Fiber Matrix Separation during Compression Molding of Fiber Reinforced Plastics; 2018.
[19] Park D-W, Oh G-H, Kim H-S. Predicting the stacking sequence of E-glass fiber reinforced polymer (GFRP) epoxy composite using terahertz time-domain spectroscopy (THz-TDS) system. Compos B Eng 2019;177:107385.
[20] Nikooharf MH, Rezaei-Khamseh M, Shirinbayan M, Fitoussi J, Tcharkhtchi AJPC. Comparison of the physicochemical, rheological, and mechanical properties of core and surface of polypropylene composite (GF50-PP) plate fabricated by thermocompression process; 2021.
[21] Renault NA, Meraghni F, Peltier L, Fitoussi J. Microstructural and experimental analysis of strain rate effect for short glass fiber reinforced polypropylene; 2015.
[22] Achour N. Modélisation multi-échelle et analyse expérimentale du comportement de composites à matrice thermoplastique renforcés fibres de verre sous sollicitations dynamiques modérées. Paris: ENSAM; 2017.
[23] Fitoussi J, Bocquet M, Meraghni F. Effect of the matrix behavior on the damage of ethylene–propylene glass fiber reinforced composite subjected to high strain rate tension. Compos B Eng 2013;45(1):1181–91.
[24] Jendli Z, Meraghni F, Fitoussi J, Baptiste D. Micromechanical analysis of strain rate effect on damage evolution in sheet molding compound composites. Compos A Appl Sci Manuf 2004;35(7–8):779–85.
[25] Jendli Z, Fitoussi J, Meraghni F, Baptiste D. Anisotropic strain rate effects on the fibre–matrix interface decohesion in sheet moulding compound composites. Compos Sci Technol 2005;65(3–4):387–93.
[26] Bonnet B. Comportement au choc de matériaux composites pour applications automobiles; 2005.
[27] Imaddahen MA, Shirinbayan M, Ayari H, Foucard M, Tcharkhtchi A, Fitoussi J. Multi-scale analysis of short glass fiber-reinforced polypropylene under monotonic and fatigue loading. Polym Compos 2020;41(11):4649–62.
[28] Arif MF, Saintier N, Meraghni F, Fitoussi J, Chemisky Y, Robert G. Multiscale fatigue damage characterization in short glass fiber reinforced polyamide-66. Compos Part B: Eng 2014;61:55–65.
[29] Shirinbayan M, Fitoussi J, Meraghni F, Surowiec B, Bocquet M, Tcharkhtchi A. High strain rate visco-damageable behavior of Advanced Sheet Molding Compound (A-SMC) under tension. Compos B Eng 2015;82:30–41.
[30] Vieira PR, Carvalho EML, Vieira JD, Toledo Filho RD. Experimental fatigue behavior of pultruded glass fibre reinforced polymer composite materials. Compos B Eng 2018;146:69–75.
[31] Shirinbayan M, Fitoussi J, Meraghni F, Surowiec B, Laribi M, Tcharkhtchi A. Coupled effect of loading frequency and amplitude on the fatigue behavior of advanced sheet molding compound (A-SMC). J Reinf Plast Compos 2017;36(4):271–82.
[32] Zhou Y, Mallick P. Fatigue performance of an injection-molded short E-glass fiber-reinforced polyamide 6, 6. I. Effects of orientation, holes, and weld line. Polym Compos 2006;27(2):230–7.
[33] Zhou Y, Mallick P. Fatigue performance of injection-molded short e-glass fiber reinforced polyamide-6, 6. II. Effects of melt temperature and hold pressure. Polym Compos 2011;32(2):268–76.
[34] Esmaeillou B, Fitoussi J, Lucas A, Tcharkhtchi A. Multi-scale experimental analysis of the tension-tension fatigue behavior of a short glass fiber reinforced polyamide composite. Procedia Eng 2011;10:2117–22.
[35] Shirinbayan M, Fitoussi J, Abbasnezhad N, Meraghni F, Surowiec B, Tcharkhtchi A. Mechanical characterization of a Low Density Sheet Molding Compound (LD-SMC): multi-scale damage analysis and strain rate effect. Compos B Eng 2017;131:8–20.
[36] Shirinbayan M, Fitoussi J, Bocquet M, Meraghni F, Surowiec B, Tcharkhtchi A. Multi-scale experimental investigation of the viscous nature of damage in Advanced Sheet Molding Compound (A-SMC) submitted to high strain rates. Compos B Eng 2017;115:3–13.
[37] Arif MF, Meraghni F, Chemisky Y, Despringre N, Robert G. In situ damage mechanisms investigation of PA66/GF30 composite: effect of relative humidity. Compos B Eng 2014;58:487–95.
[38] Rolland H, Saintier N, Robert G. Damage mechanisms in short glass fibre reinforced thermoplastic during in situ microtomography tensile tests. Compos B Eng 2016;90:365–77.
[39] Rolland H, Saintier N, Raphael I, Lenoir N, King A, Robert G. Fatigue damage mechanisms of short fiber reinforced PA66 as observed by in-situ synchrotron X-ray microtomography. Compos B Eng 2018;143:217–29.
[40] Sun B, Li Z. A multi-scale damage model for fatigue accumulation due to short cracks nucleation and growth. Eng Fract Mech 2014;127:280–95.
[41] Sun B, Xu Y-L, Li Z. Multi-scale fatigue model and image-based simulation of collective short cracks evolution process. Comput Mater Sci 2016;117:24–32.
[42] Sun B, Xu Y-L, Li Z. Multi-scale model for linking collective behavior of short and long cracks to continuous average fatigue damage. Eng Fract Mech 2016;157:141–53.
[43] Sun B. A continuum model for damage evolution simulation of the high strength bridge wires due to corrosion fatigue. J Constr Steel Res 2018;146:76–83.
[44] Nobelen M, Hayes BS, Seferis JC. Cryogenic microcracking of rubber toughened composites. Polym Compos 2003;24(6):723–30.
[45] Shirinbayan M. Multiscale damage analysis of the tension-tension fatigue behavior of a low-density sheet molding compound. J Appl Polym Sci 2021;138(4):49721.
[46] Sun B, Zheng Y, Li Z. A multi-scale corrosion fatigue damage model of aluminum alloy considering multiple pits and cracks. Acta Mech Solida Sin 2018;31(6):731–43.